



Adiabatic shear banding in plane strain tensile deformations of 11 thermoelastoviscoplastic materials with finite thermal wave speed

R.C. Batra ^{*}, M.H. Lear

Department of Engineering Science and Mechanics, MC 0219, Virginia Polytechnic Institute and State University, Blacksburg, VA 24061, USA

Received in final revised form 21 July 2004

Available online 6 November 2004

Abstract

We study the initiation and propagation of adiabatic shear bands (ASBs) in 11 homogeneous materials each modeled as microporous, isotropic and thermoelastoviscoplastic, and deformed in plane strain tension. The heat conduction in each material is assumed to be governed by a hyperbolic heat equation; thus thermal and mechanical waves propagate with finite speeds. The decrease in the thermophysical parameters due to the increase in porosity is considered. An ASB is assumed to initiate at a material point when the maximum shear stress there has dropped to 80% of its peak value for that material point and it is deforming plastically. An approximate solution of the coupled nonlinear partial differential equations subject to suitable initial and boundary conditions is found by the finite element method (FEM). In contrast to the Considère and the Hart criterion, it is found that an ASB initiates when the axial load drops rapidly and not when it peaks. The refinement of the 40×40 uniform FE mesh to 120×120 uniform elements decreased the ASB initiation time by 2.1% while increasing the CPU time by a factor of ~ 26 . By locating points where the ASB has initiated we find its current length, width and speed. The 11 materials are ranked according to the time of initiation of an ASB under otherwise identical geometric and loading conditions with the same

^{*} Corresponding author. Tel.: +1 540 2316051; fax: +1 540 2314574.

E-mail addresses: rbatra@vt.edu (R.C. Batra), learnh1@jhuapl.edu (M.H. Lear).

initial nonuniform porosity distribution. This ranking of materials is found to differ somewhat from that ascertained by Batra and Kim (1992) who studied simple shearing deformations, and by Batra et al. (1995) who analyzed three-dimensional torsional deformations of thin-walled tubular specimens. The average axial strain determined from the maximum axial load condition differs noticeably from that when an ASB initiates.

© 2004 Elsevier Ltd. All rights reserved.

Keywords: Adiabatic shear band speed; Instability criteria; Ranking of 11 materials according to ASB susceptibility; Porosity; Stress triaxiality ratio

1. Introduction

Tresca (1878) and Massey (1928) observed hot lines, now called adiabatic shear bands (ASBs), in the form of an X during the hot forging of a rectangular platinum bar. By coating metals with wax and monitoring patterns and the extent of melting, Tresca (1878, p. 316) concluded that at least 70% of the plastic working was converted into heating. Subsequently, Taylor and Quinney (1934) found that, depending upon the material, this factor equalled 85–95%. Recently, Mason et al. (1994) have asserted that the fraction of plastic working converted into heating depends upon the plastic strain and the plastic strain rate. Research activity in ASBs picked up since Zener and Hollomon (1944) observed them during the punching of a hole in a steel plate. They stated that a material point becomes unstable when softening of the material caused by its temperature rise overcomes its hardening due to strain and strain-rate effects. Heat conduction is a slow process; thus under high rates of deformation there is not enough time for the heat produced at a point to be conducted away. The softened material within the heated zone is deformed even more during further deformations of the body resulting in a catalytic process, which eventually ends with deformations of the material becoming unstable. Whereas heat conduction plays a negligible role until the time of initiation of an ASB, its role is significant during the development and propagation of an ASB (e.g., see Batra and Kim (1991) and Batra and Chen (2001a)). Batra (1987a,b) has delineated the effect of different material parameters on the initiation and development of ASBs. We note that ASBs have also been observed in high speed machining (e.g., see Molinari et al. (2002); Burns and Davies (2002)). Schoenfeld and Kad (2002) analyzed material plugging in Ti–6Al–4V plates.

Considerè (1885) postulated that, under static deformations, a structure becomes unstable when the load supported by it reaches a maximum value. For simple shearing deformations, it is equivalent to the shear stress attaining a maximum value at the time of instability. Recht (1964) and Clifton (1980) used this criterion to find the nominal strain when a thermoviscoplastic material becomes unstable. Bai (1982, Eq. (4.1) or (4.3)) found the instability strain by examining the stability of a homogeneous solution of equations governing the transient simple shearing deformations of a thermoviscoplastic body. Batra and Chen (2001b) and Wei and Batra (2002) have shown that the Considerè criterion and the Bai criterion give essentially

the same value of the instability strain for simple shearing deformations of a thermo-viscoplastic body. Lindholm and Johnson (1983) calculated the instability shear strain for 12 materials by using the Considère criterion and the Johnson-Cook (1983) relation for the dependence of the flow stress upon the plastic strain, the plastic strain-rate and the temperature. Batra et al. (1995) studied three-dimensional (3-D) torsional deformations of a thin-walled tube and ranked these 12 materials according to the nominal strain at the time of initiation of a shear band as signified by a sudden drop in the torque required to deform the tube. Batra and Kim (1992) had earlier analyzed transient simple shearing deformations of the same 12 materials, introduced an initial geometric defect to make deformations inhomogeneous and proposed that an ASB initiates at a point when the shear stress there has dropped to 80% of its peak value at that point and the material point is deforming plastically. The motivation for this ansatz was the experimental work of Marchand and Duffy (1988) that showed a drop in the torque required to deform a thin-walled tube once an ASB had initiated. The ranking of materials according to the nominal shear strain at the initiation of an ASB found by Batra and Kim (1992) matched with that determined by Lindholm and Johnson (1983). Batra and Kim (1992) also computed the band width as a function of the defect size, the localized strain within an ASB, and the temperature rise in the ASB. Molinari and Clifton (1987), amongst others, have characterized the effect of the defect size upon the ASB initiation. Besides the 3-D work of Batra et al. (1995) cited above, Zbib and Jubran (1992), Batra and Zhang (1994), Batra and Ravisankar (2000) and Batra and Wang (2004) have analyzed 3-D deformations to study ASBs. The latter two studies found that an ASB initiated on the midsurface of a dynamically loaded prenotched plate considerably earlier than it initiated on the front or the back surface. Furthermore, the ASB initiation time predicted by the plane strain analysis is much smaller than that given by the 3-D solution of the same problem.

For an axially loaded body changes in the area of cross-section should be considered when applying Considère's (1885) maximum load criterion to find the axial strain at the onset of instability. Hart (1967) also accounted for the variation of the strain-rate during the loading process. Here, we assume that deformations are locally adiabatic, and augment Hart's work with the consideration of temperature rise due to plastic working. The instability strain thus determined is compared with the ASB initiation strain for the 11 materials studied here.

Much of the work on ASBs can be found in special issues of the *Mechanics of Materials* edited by Armstrong et al. (1994), the *Applied Mechanics Reviews* edited by Zbib et al. (1992), the *International Journal of Fracture* edited by Batra et al. (2000), and books *Material Instability* edited by Batra and Zbib (1994), *Localization and Fracture Phenomenon in Inelastic Solids* edited by Perzyna (1998), and books authored by Bai and Dodd (1992) and Wright (2002). Nearly all works on 2- and 3-D analysis of ASBs have been numerical. Exceptions include the study on the asymptotic structure of ASBs in antiplane shear deformations by Wright and Walter (1996) and in mode-II deformations by Chen and Batra (1999a). They assumed that an ASB propagates with a uniform velocity, it can be represented as a singular surface and deformations appear steady to an observer situated on the ASB tip. These

are simplifying assumptions as an ASB has a finite width, and the 3-D numerical study of the shear band propagation speed in torsional deformations of a thin-walled tube by [Batra and Zhang \(1994\)](#) revealed that the shear band speed increased as it propagated along the circumference of the tube. The ASB speed, defined as the speed of propagation of a contour of the effective plastic strain of 1.0, increased with an increase in the nominal strain rate. Except for the torsional problem, the speed of an ASB depends upon the value of the effective plastic strain at which an ASB is assumed to initiate (e.g., see [Needleman \(1989\)](#) and [Zhu and Batra \(1991\)](#)). Whereas works cited thus far have assumed the body to be homogeneous, [Charalambakis and Baxevanis \(2004\)](#) and [Batra and Love \(2004\)](#) have analyzed ASBs in an inhomogeneous body.

Here, we analyze plane strain tensile deformations of a microporous thermoelastoviscoplastic body. Most of the experimental and numerical studies on ASBs have not explicitly defined the criterion employed for the initiation of an ASB. Following [Batra and Kim \(1992\)](#), we assume that an ASB initiates at a point when the maximum shear stress there has dropped to 80% of its peak value and the material point is deforming plastically. The latter condition rules out the initiation of an ASB during elastic unloading. By locating the tip of a propagating ASB as a function of time, we find its width, length and speed. A distinguishing feature of the present work from earlier 2-D studies is the use of a hyperbolic rather than a parabolic heat equation. Thus thermal disturbances like mechanical perturbations propagate with a finite speed. [Batra and Chen \(2001b\)](#) concluded that the spacing among adjacent ASBs depends upon the thermal wave speed only when it equals a few m/s; otherwise results are essentially the same as those for the infinite wave speed admitted by a parabolic heat equation. [Saad and Cha \(1982\)](#) found that in heat transfer problems involving very brief time intervals of about $10 \mu\text{s}$ and/or very high fluxes of the order of 10^5 W/cm^2 , results obtained from the hyperbolic and the parabolic heat equations are quite different. [Chandrasekharai \(1986\)](#) has reviewed much of the literature on hyperbolic heat equations. [Batra \(1975\)](#) considered higher-order spatial and temporal derivatives of temperature and found that constitutive relations compatible with the Clausius–Duhem inequality admitted the feasibility of thermal disturbances propagating with a finite speed; however, for such materials, either a linear problem has a unique solution or thermal waves propagate at a finite speed. Ideally, one will like to have both.

Under identical plane strain loading conditions and initial nonuniform distribution of porosity, we analyze the problem for 11 materials whose torsional or simple shear deformations were studied by [Lindholm and Johnson \(1983\)](#), [Batra and Kim \(1992\)](#), and [Batra et al. \(1995\)](#); [Batra \(1998\)](#) has summarized some of these studies. We find the time of initiation of an ASB, its speed of propagation, and rank these materials according to their susceptibility to adiabatic shear banding defined as the average axial strain at the instant of the initiation of an ASB. For two materials, we also study the influence on the ASB initiation and propagation of the thermal conductivity, and for one material the effect of the nominal strain rate. [Batra and Jin \(1994\)](#) studied plane strain tensile deformations of a steel specimen with a Liton-ski–Batra (e.g., see [Batra \(1988a,b\)](#)) thermoviscoplastic relation and a parabolic heat

equation. They showed that the porosity induced softening is more significant than thermal softening.

The paper is organized as follows. Section 2 lists assumptions made in analysing the problem. Computed results are described and discussed in Section 3, and conclusions are summarized in Section 4.

2. Formulation of the problem

The balance laws for mass, linear momentum, moment of momentum, and the internal energy, are written in the Lagrangean or the referential description of motion. Elastic deformations, heat conduction and stresses due to thermal expansion are considered. Following assumptions are made in the analysis of the problem: (i) the strain-rate tensor is additively decomposed into an elastic part, a plastic part and a thermal part, (ii) the Jaumann rate of the Cauchy stress tensor is a linear function of the elastic part of the strain-rate tensor; (iii) Young's modulus and the shear modulus decrease affinely to zero when the porosity approaches one; (iv) the porosity represents damage induced in the body; (v) the specific heat and the thermal conductivity are affine functions of porosity; (vi) a material point deforms plastically when the stress state satisfies [Gurson's \(1977\)](#) flow potential modified by [Tvergaard and Needleman \(1984\)](#) for its dependence upon the porosity and the dependence of the flow stress upon the plastic strain, plastic strain rate and temperature; the latter is assumed to be given by the [Johnson-Cook \(1983\)](#) relation; (vii) the associative flow rule of plasticity gives the plastic part of the strain-rate tensor; (viii) [Chu and Needleman's \(1980\)](#) expression for the evolution of porosity applies; (ix) the rate of change of internal energy is a linear function of the first and the second time derivatives of temperature thereby resulting in a hyperbolic heat equation due to [Vernotte \(1958\)](#); thus both mechanical and thermal disturbances propagate at finite speeds, (x) the body is homogeneous and isotropic and (xi) the body is prismatic of uniform square cross-section of side $2H$, initial and boundary conditions are independent of the axial coordinate, and a plane strain state of deformation prevails in the body. A complete set of equations and values of material variables used in computing results are given in [Lear \(2003\)](#). [Batra and Lear \(2004\)](#) have used these equations to study the initiation and propagation of brittle and ductile failures in an impact loaded prenotched plate. They simulated the crack opening by the nodal release technique and found the speed of crack due to brittle failure to equal 28% of the Rayleigh wave speed. [Batra and Love \(2004\)](#) have used these equations to study the initiation and propagation of ASBs in a functionally graded body.

An equal and opposite axial velocity is applied to the smooth top and bottom surfaces; this velocity increases linearly from zero to its final value V_0 in $1 \mu\text{s}$ and is then held constant thereby giving an average strain rate of V_0/H . The thermomechanical deformations are assumed to be symmetric about the two centroidal axes. Thus deformations of material in the first quadrant are analyzed with boundary conditions arising from the symmetry of deformations imposed at points on the vertical and the horizontal centroidal axes. The other vertical and the horizontal surfaces are taken

to be traction free and thermally insulated. The body is initially at rest and at a uniform temperature.

3. Computation and discussion of results

A FE computer code employing 4-node isoparametric quadrilateral elements and 2×2 integration rule has been developed to find an approximate solution of the above formulated initial-boundary-value problem. The coupled ordinary differential equations resulting from the semidiscrete formulation of the problem are integrated with the subroutine LSODE (Livermore Solver for Ordinary Differential Equations). It adjusts the time step adaptively to compute the solution within the prescribed absolute and relative tolerances; each tolerance was set equal to 10^{-5} . It has been found that the time step chosen by LSODE decreases rapidly when the deformation begins to localize at one or more points in the body as indicated by the drop in the maximum shear stress at these points while they are deforming plastically.

The plane strain thermomechanical problem analyzed here is similar to that studied by [Batra and Jin \(1994\)](#) and [Batra and Jaber \(2001\)](#) with the following two exceptions: We employ a hyperbolic heat equation instead of a parabolic one, and we use 4-node quadrilateral elements and they employed 3-node constant strain triangular elements. [Batra and Jin \(1994\)](#) adaptively refined the spatial mesh in which the size of an element generated was inversely proportional to the effective strain rate (or any other scalar measure of deformation) at the element centroid. [Batra and Jaber \(2001\)](#) integrated constitutive relations at the centroid of each triangular element, which reduces the number of unknowns. Both in their and in the present work, coordinates of nodes are updated after every time increment.

The developed code was validated by solving several simple problems with thermal relaxation time $\tau = 0$ and comparing the computed solution with that found from the earlier code of [Batra and Jin \(1994\)](#). For $\tau > 0$, a heat conduction problem was solved for a nonporous rigid body and the computed speed of the thermal wave was found to match well with the analytical value. Finally, for $\tau = 0$, a shear band problem analyzed previously by [Batra and Jin \(1994\)](#) was solved with the present code; the two sets of computed results were found to match well. The computer code can also be verified by using the method of manufactured solutions in which body forces and sources of internal energy density can be found for any assumed deformation and temperature fields. These and initial and boundary conditions corresponding to the assumed solution are input into the code. The computed solution should match the presumed analytical solution of the problem (e.g., see [Batra and Liang \(1997, Eq. \(30\)\)](#) and a few lines following it).

We have studied the initiation and propagation of ASBs in 11 materials; values of thermomechanical parameters for these materials are listed in [Batra and Kim \(1992\)](#). The quarter of the cross-section is divided into 3600 uniform 4-node square elements.

For the homogeneous body with uniform initial conditions, deformations will become inhomogeneous because of the interaction with the incident waves of waves reflected from the boundaries and corners. This may happen at different instants in the

11 materials because of the differences in their material properties. In order to ensure some kind of uniformity, an initial defect in the form of a nonuniformly distributed initial porosity, f_0 , given by

$$f_0(\mathbf{X}, 0) = f_{ce} \left(1 - \left(\frac{R}{H} \right)^2 \right)^9 e^{-5(R/H)^2} \quad (1)$$

is introduced. Here f_{ce} is the initial porosity at the specimen centroid and may be thought of as representing the strength of the defect, and R is the distance, from the origin, of the material point at place \mathbf{X} . In the following discussion, initial porosity distributions with $f_{ce} = 0.025$ and 0.05 are referred to as weak and strong defects, respectively. Results for one material are computed for several values of the thermal relaxation time, τ , to delineate the effect of the thermal wave speed on the initiation of an ASB. Otherwise, τ is set equal to 10^{-8} s.

3.1. Adiabatic shear band initiation criterion

We follow [Batra and Kim's \(1992\)](#) criterion and assume that an ASB initiates at a point when

$$\tau_{\max} = 0.8\tau_{\text{peak}} \quad \text{and} \quad \dot{\epsilon}_e^p > 0, \quad (2)$$

where τ_{\max} is the maximum shear stress at that point, τ_{peak} is the peak value of τ_{\max} reached at that point, and $\dot{\epsilon}_e^p$ is the effective plastic strain rate. The accompanying condition, $\dot{\epsilon}_e^p > 0$, ensures that the drop in the maximum shear stress is due to softening of the material and not due to elastic unloading. The necessity of the requirement $\dot{\epsilon}_e^p > 0$ is illustrated by the plots in [Fig. 1](#) of the time histories of τ_{\max} and $\dot{\epsilon}_e^p$ at two material points in the 4340 steel specimen – one within (point W) an ASB and the other outside (point P) of an ASB. Even though τ_{\max} has dropped to 80% of its maximum value at each point, the effective plastic strain stops growing at point P but its rate of increase picks up at point W when τ_{\max} begins to decrease at each point. The rapid increase in $\dot{\epsilon}_e^p$ signifies the onset of the localization of deformation at point W and $\dot{\epsilon}_e^p = 0$ for elastic unloading at P . Thus an ASB initiates at the point W at the nondimensional time $\bar{t} = tV_0/H = 0.325$. [Batra and Rattazzi \(1997\)](#) studied the initiation of an ASB at the root of a V-notch in a thick-wall steel tube and found that the ASB initiation criterion noticeably affects the computed results. Because of the forward-difference time integration scheme and the rather coarse FE mesh employed, [Wright and Batra \(1985\)](#) did not see a precipitous drop in the shear stress associated with the initiation of an ASB.

3.2. Effect of FE mesh

In order to quantify the effect of the FE mesh on the ASB initiation time, we computed results [Batra and Love \(in preparation\)](#) with three uniform meshes for a tungsten heavy alloy under otherwise identical conditions. As is clear from the results summarized in [Table 1](#), the ASB initiation time decreased by only 2.1% in going

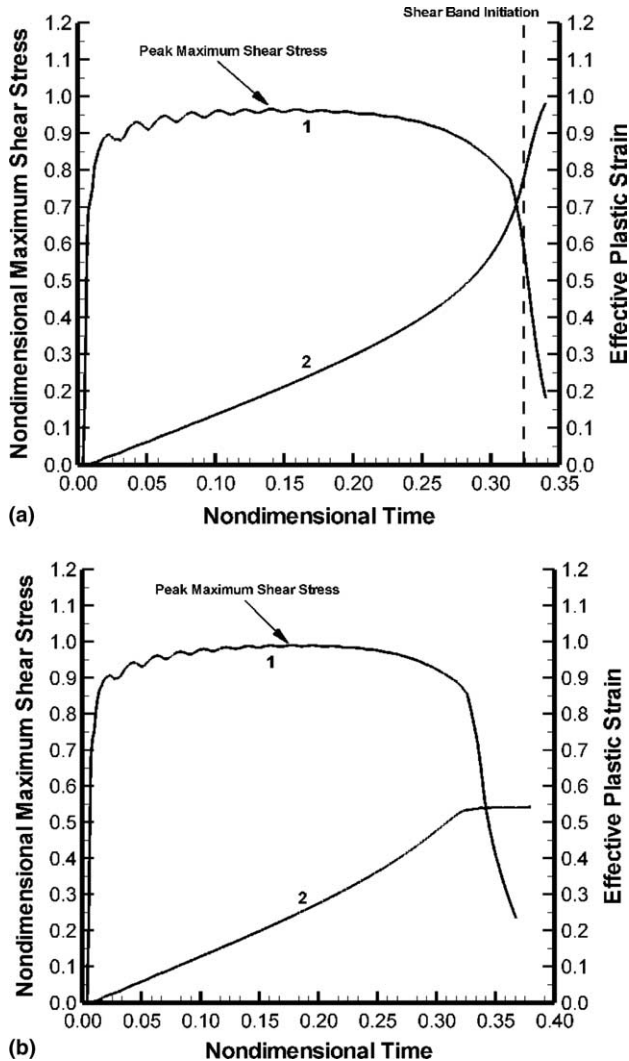


Fig. 1. Time histories of the effective plastic strain and the maximum shear stress at two material points *W* and *P* in a 4340 steel specimen; Fig. 1(a) is for point *W* within an ASB, and Fig. 1(b) is for point *P* outside of an ASB.

from a 40×40 to 120×120 uniform mesh. Recalling that the width of a typical ASB is $10 \mu\text{m}$, one needs 25×10^6 uniform elements in a $5 \text{ mm} \times 5 \text{ mm}$ specimen to fully resolve the band. The use of a properly graded mesh will reduce the number of elements. However, it requires a priori knowledge of the location and the direction of propagation of the ASB. At present, we do not have sufficient computational resources to perform the calculation. However, as the above-mentioned exercise shows, the 60×60 uniform mesh gives the ASB initiation time within 2% accuracy.

Table 1

Effect of FE mesh on the ASB initiation time for a tungsten heavy alloy deformed in plane strain tension at a nominal strain rate of 5000/s

Uniform FE mesh	ASB initiation time (μs)	CPU time (s)	% Change in ASB initiation time
40 \times 40	65.9	1133	–
80 \times 80	64.8	6908	1.67
120 \times 120	64.5	29,242	2.12

The time histories of the evolution of the maximum shear stress for a structural steel computed with 60 \times 60, 80 \times 80 and 120 \times 120 uniform FE meshes essentially overlapped each other until the maximum shear stress begins to drop rapidly or equivalently an ASB initiates. The ASB initiation time computed with the three FE meshes equalled 54, 53.6 and 53.4 μs , respectively.

3.3. Effect of thermal wave speed

For the 4340 steel and the weak defect, results have been computed for the thermal relaxation time $\tau = 0, 10^{-8}, 10^{-7}, 10^{-6}, 10^{-5}$ and 10^{-4} s; corresponding speeds of a thermal wave equal $\infty, 31.88, 10.08, 3.19, 1.01$ and 0.32 m/s, respectively. Note that the thermal wave speed is inversely proportional to $\sqrt{\tau}$. For several values of time, \bar{t} , the criterion (2) for the initiation of an ASB was applied at the centroid of every element in the problem domain thus enabling us to determine when and where the ASB initiated. The time history of the length of the ASB so ascertained for the six values of τ and the weak initial defect is plotted in Fig. 2(a) and Fig. 2(b) exhibits these time histories for three uniform FE meshes. The slopes of these curves equal the ASB speed; we note that slopes of curves in Fig. 2(b) are nearly equal. The ASB length has been non-dimensionalized by $H = 5$ mm. The final ASB speed is computed at the instant when the porosity at the centroid of the specimen equals 0.2. The three curves for $\tau = 0, 10^{-8}$ and 10^{-7} s are very close to each other signifying that for $\tau \leq 10^{-7}$ s, the ASB initiation time and speed are virtually unaffected. However, as τ is increased which results in lower speeds of thermal waves, the initiation of the ASB is delayed and its propagation speed is lowered; the initial and the final ASB speeds are listed in Table 2. This may be illustrated by setting thermal conductivity $\kappa = 0$ in the balance of internal energy which then becomes analogous to the equation of motion of a unit mass attached to a damper of viscosity $1/\tau$. With a decrease in τ for this system, it takes a little longer for the temperature to reach its final value at a point. It is clear that for $\tau \leq 10^{-6}$ s, the final ASB speed is nearly 2.3 times its initial speed. For torsional deformations of a thin-walled steel tube deformed at an average shear strain rate of 5000/s, Batra and Zhang (1994) found that the ASB increased from 180 m/s at the time of initiation of an ASB to 1130 m/s when the ASB reached the diametrically opposite point. They took $\tau = \kappa = 0$, so there was neither heat conduction nor a thermal wave.

Marchand and Duffy (1988) computed the shear band speed from their test observations to be 250 m/s in a high strength steel. Zhou et al.'s (1996a) test results

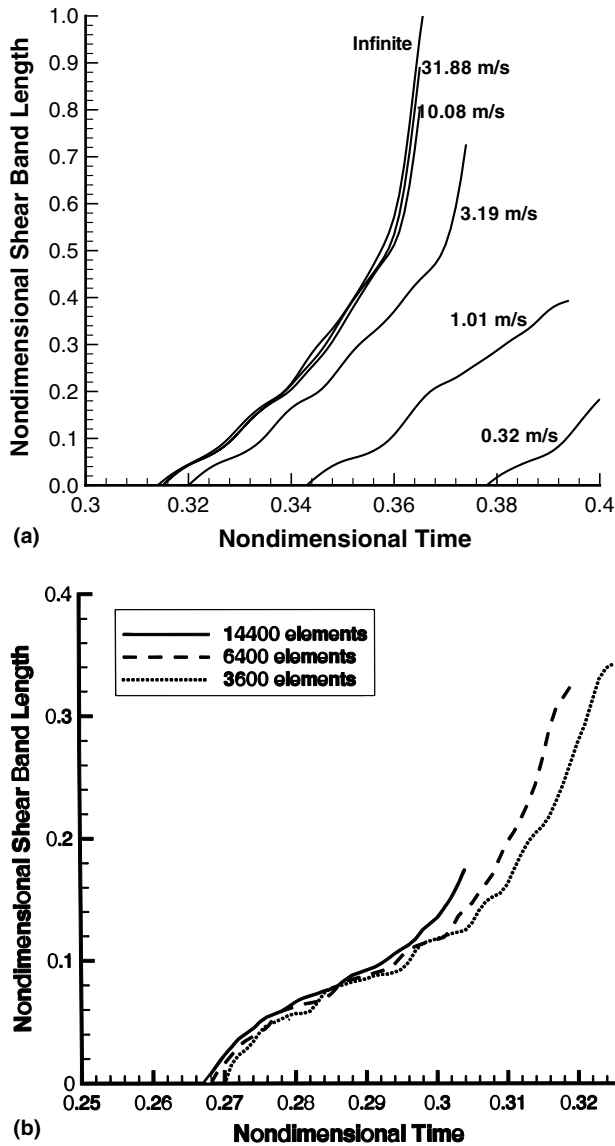


Fig. 2. (a) Time histories of the ASB length for six values of the thermal wave speed and the weak defect at the specimen centroid. (b) Time histories of the ASB length for three uniform FE meshes.

indicated that the ASB speed increased with time to a maximum of around 1 km/s in a HY-100 steel. [Batra and Rattazzi \(1997\)](#) found that the computed speed strongly depends upon the thermal softening characteristics of the material. They analyzed the propagation of an ASB during torsional deformations of a thick-walled tube with a circumferential V-notch, and found that the affine thermal softening in the

Table 2

For the 4340 steel and the weak defect, the initial and the final speeds of propagation of an ASB as a function of the thermal relaxation time

Thermal relaxation time (s)	0	10^{-8}	10^{-7}	10^{-6}	10^{-5}	10^{-4}
Thermal wave speed (m/s)	∞	31.88	10.08	3.19	1.01	0.32
Avg. axial strain when ASB initiates	0.314	0.315	0.315	0.320	0.343	0.378
Initial speed of an ASB (m/s)	144	135	144	145	147	133
Final speed of an ASB (m/s)	318	318	318	347	299	336

Johnson-Cook relation gave an ASB speed of about 250 m/s and the power law thermal softening in the thermoviscoplastic relation used by Zhou et al. (1996b) gave an ASB speed of about 1 km/s. The Johnson-Cook relation is based on torsional tests conducted at moderate strain rates and temperatures; its validity for strains, strain rates and temperatures occurring in an ASB has not been established since there is very little test data at these deformation levels. One reason for not achieving a steady speed of ASBs during our computations is that the ASB has to travel a small distance before the effect of free boundaries becomes significant. After the ASB has reached nearly half way between the centroid and the free right surface, deformations at points on the free boundary where the ASB will intersect it begin to localize and an ASB starts to propagate inwards from there. For example, the width of the specimen in the necked region is 3.5 mm and the maximum distance an ASB can traverse is about 5.3 mm. Bonnet-Lebouvier et al. (2002) have analyzed plane strain thermo-mechanical deformations of a 200 mm \times 2.5 mm layer with periodic boundary conditions at the edges $x = 0$ and $x = 200$ mm, a geometric defect at the point (0, 1.25) aligned along the x -axis, and equal and opposite tangential velocities prescribed on the surfaces $y = \pm 1.25$ mm. They did not report the ASB initiation criterion. For CRS1018 steel, the ASB speed vs. the nominal strain rate reported in Fig. 5 of their paper implies that the ASB speed increases with an increase in the nominal strain rate. For a nominal strain rate of 5000/s, the computed ASB equalled about 180 m/s and approached a steady value of approximately 800 m/s for nominal strain rates exceeding 1.2×10^5 /s. The size of the smallest element in the mesh was decreased as the nominal strain rate increased.

Whereas we have found the ASB by locating its tip at different instants, previous numerical studies (e.g., see Needleman (1989) and Zhu and Batra (1991)) determined it from contours of the effective plastic strain. In general, the ASB speed will depend upon the level of the contour or the ASB initiation criterion. However, for the 3-D torsion of a thin-walled tube analyzed by Batra and Zhang (1994), the computed ASB speed seemed not to depend upon the level of the contour of the effective plastic strain.

Fig. 3 exhibits time histories of the evolution of the maximum shear stress at the centroid of the cross-section. The curves are qualitatively similar for each of the six values of τ . When the state of deformation at the centroid satisfies the ASB initiation criterion (2), the maximum shear stress there begins to collapse. The rate of collapse of the maximum shear stress is virtually unaffected when τ is decreased from 10^{-7} to zero.

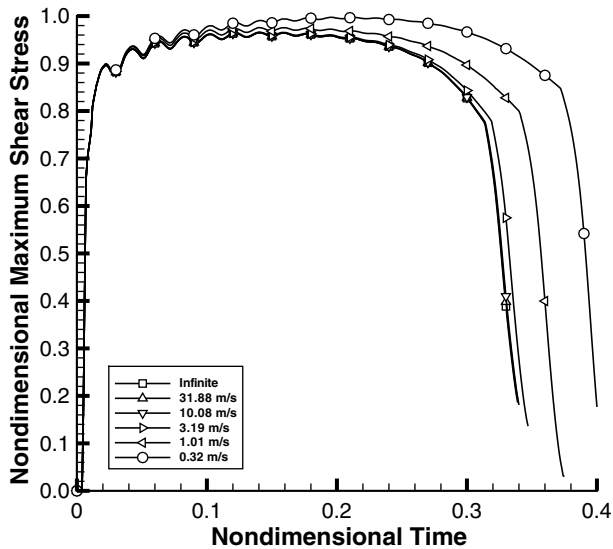


Fig. 3. For six thermal wave speeds, time histories of the evolution of the maximum shear stress.

3.4. Effect of defect size

For each one of the 11 materials studied, computed time histories of the length of an ASB with $\tau = 10^{-8}$ s and for the weak and the strong defects are exhibited in Fig. 4(a) and (b). It is clear that the strength of the defect does not alter the ordering of materials according to the time of initiation of an ASB; however, the time history of the evolution of its length and hence the speed of propagation are noticeably influenced by the defect size. For doubling of the defect strength, the average axial strain at the time of initiation of an ASB drops to about 2/3 of its value for the weak defect for each one of the eleven materials, and for Depleted Uranium, Tungsten and S-7 tool steel, the final ASB speed is considerably higher than the initial ASB speed. For the weak defect, the homologous temperature (defined as the ratio of the current temperature to the melting temperature of the material) at the instant of ASB initiation varies from a low of 0.03 for Armco iron to 0.24 for 2024 Aluminum. This depends upon the yield stress of the material, the strain at the instant of the initiation of an ASB, and the heat capacity of the material. For the weak defect, the ratio of the average axial strain at the instant of the initiation of an ASB to that when the maximum shear stress peaks has the lowest value of 1.32 for the cartridge brass and the highest value of 5.7 for the tungsten. The ratio of the corresponding values of the effective plastic strain for the two materials equals 1.43 and 14.8, respectively.

3.5. Stress triaxiality ratio

The stress triaxiality ratio, defined as $\sigma_{kk}/3\sigma_{22}$, (σ is the Cauchy stress tensor) at the specimen centroid has the lowest value of 1.06 for 7039 Aluminum and Armco

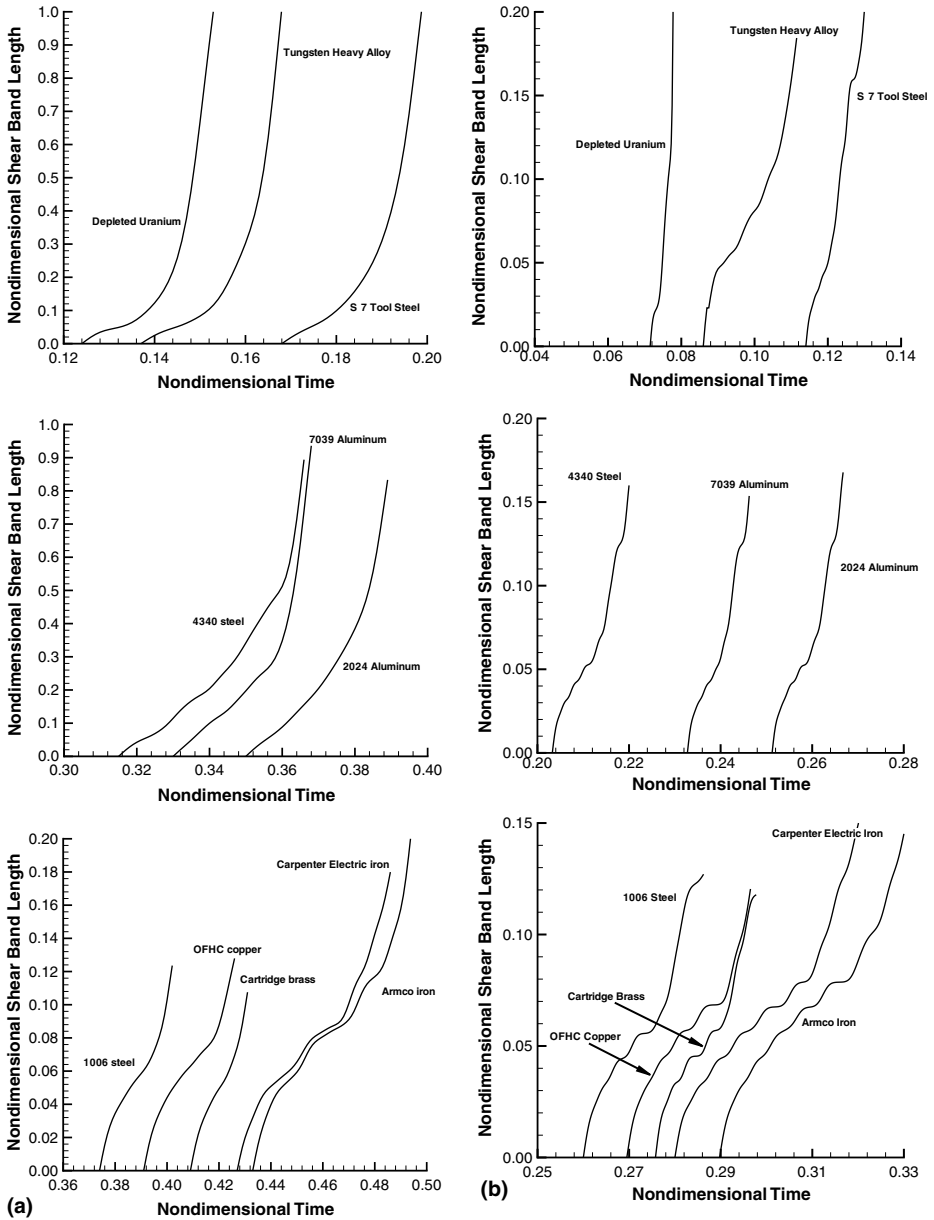


Fig. 4. For the eleven materials studied, time histories of the length of an ASB for (a) the weak, and (b) the strong defects.

iron and the highest value of 1.43 for depleted Uranium. Vandergiessen et al. (1995) have suggested that higher values of the triaxiality factor enhance the nucleation of voids. Here the stress-controlled nucleation of voids has not been considered.

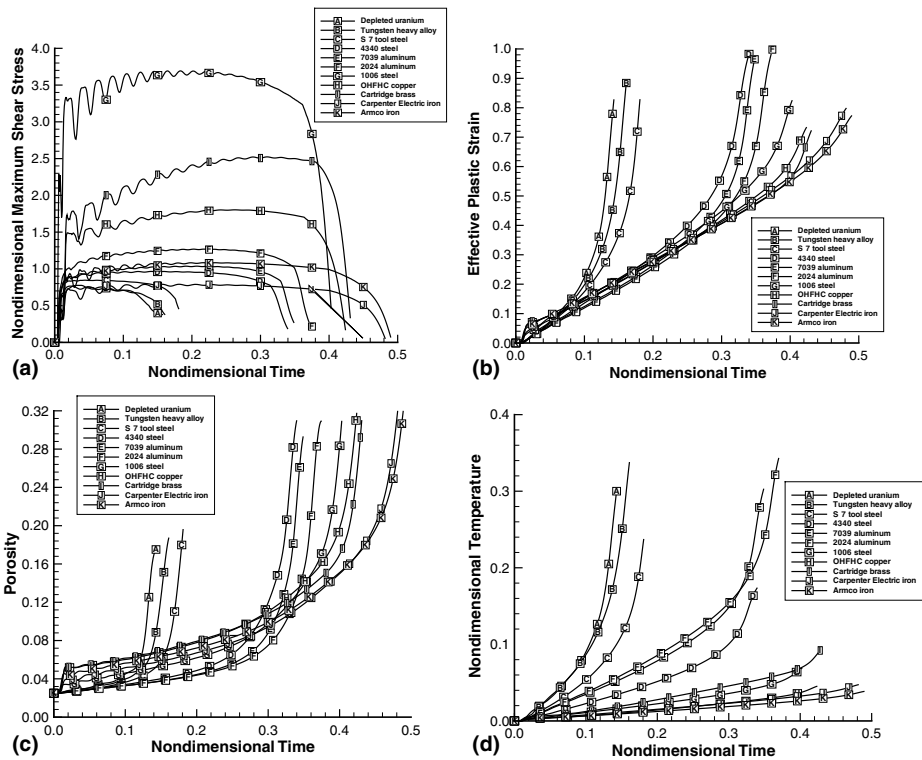


Fig. 5. For each one of the eleven materials studied, time histories of the evolution of (a) the maximum shear stress, (b) the effective plastic strain, (c) the porosity, and (d) the temperature at the centroid of the cross-section.

However, the triaxiality influences the development of the yield surface and the evolution of plastic strain rates. [Batra and Ravisankar \(2000\)](#) studied the initiation and propagation of an ASB from a notch tip in an impact loaded prenotched nonporous plate and found that $\sigma_{ii} < 0$ within an ASB.

3.6. Ranking of the 11 materials according to the ASB initiation time

We have listed in [Table 3](#), the ranking of the 11 materials according to the times of initiation of an ASB and also the computed initial and the final speeds of propagation of the ASB. Note that the nondimensional time equals the average axial strain. In [Table 3](#), we have also listed the axial instability strain, ε_i , determined from the Considère condition $d\sigma_y/d\varepsilon_c^p = \sigma_y$, where σ_y is the flow stress of the material. Assuming that $d\dot{\varepsilon}_c^p/d\varepsilon_c^p = 0$, $\dot{\varepsilon}_c^p = 5000/s$, elastic deformations and the heat conduction effects are negligible, $\tau = 0$, $d\theta = \sigma_y d\varepsilon_c^p / \rho c$, and the specimen is deformed in simple tension, ε_i is given by

Table 3

For the eleven materials, values of the nominal axial strain, the effective plastic strain, and the homologous temperature when the maximum shear stress peaks and when an ASB initiates

Material	Effective strain from		Weak defect							Strong defect				
			τ_{\max} has peak value			When ASB initiates				ASB speed (m/s)		Axial strain when ASB initiates		ASB speed (m/s)
	Considerè's condition	Hart's criterion	Axial strain	Effective plastic strain	Homologous temperature	Axial strain	Effective plastic strain	Homologous temperature	Triaxiality ratio	Initial	Final	Initial	Final	Initial
Depleted uranium	0.0498	0.0495	0.038	0.0527	0.0216	0.124	0.4091	0.1598	1.430	124	496	0.072	193	334
Tungsten	0.0045	0.004422	0.024	0.0283	0.0123	0.137	0.4180	0.1757	1.255	140	648	0.086	165	357
S-7 tool steel	0.0173	0.01709	0.044	0.0567	0.0169	0.168	0.5468	0.1627	1.147	157	517	0.114	247	357
4340 steel	0.0491	0.0485	0.141	0.1980	0.0337	0.315	0.6794	0.1201	1.069	158	214	0.203	239	399
7039 aluminum	0.0818	0.0810	0.207	0.2750	0.0821	0.330	0.6860	0.2127	1.056	235	244	0.233	265	355
2024 aluminum	0.1013	0.1002	0.218	0.2810	0.0958	0.350	0.6806	0.2433	1.071	183	184	0.251	265	418
1006 steel	0.0782	0.0764	0.183	0.2660	0.0204	0.374	0.6406	0.0525	1.117	98	42	0.260	198	46
OFHC copper	0.1810	0.1765	0.262	0.3612	0.0198	0.391	0.5886	0.0351	1.081	107	45	0.270	206	26
Cartridge brass	0.2649	0.2628	0.310	0.4187	0.0476	0.409	0.5951	0.0742	1.108	102	52	0.276	207	82
Carpenter electric iron	0.1194	0.1142	0.181	0.2566	0.0138	0.427	0.6208	0.0359	1.093	105	22	0.280	199	92
Armco iron	0.1579	0.1516	0.222	0.2998	0.0134	0.433	0.6099	0.0295	1.061	189	79	0.290	198	76

Values of the triaxiality ratio at the specimen centroid and the speed of an ASB are also listed.

$$\frac{nB\dot{\epsilon}_i^{n-1}}{A + B\dot{\epsilon}_i^n} - \frac{(A + B\dot{\epsilon}_i^n)(1 + C \ln(\dot{\epsilon}_i/\dot{\epsilon}_0))}{\theta_m \rho c} = 1. \quad (3)$$

Here $A, B, n, \dot{\epsilon}_0$ and C are material parameters in the Johnson-Cook (1983) relation, ρ is the mass density and c the specific heat. Hart (1967) accounted for the variation of the axial strain rate during the loading process. For a bar pulled at a uniform axial speed and assuming that deformations are locally adiabatic, an instability occurs when

$$1 = \frac{1}{\sigma_y} \frac{\partial \sigma_y}{\partial \epsilon} \dot{\epsilon} + \frac{1}{\rho c} \frac{\partial \sigma_y}{\partial \theta} - \frac{1}{\sigma_y} \ddot{\epsilon} \frac{\partial \sigma_y}{\partial \dot{\epsilon}}, \quad (4)$$

which for the Johnson-Cook relation reduces to

$$\frac{Bn\dot{\epsilon}_i^{n-1}}{A + B\dot{\epsilon}_i^n} - \frac{(A + B\dot{\epsilon}_i^n)(1 + C \ln(\dot{\epsilon}_i/\dot{\epsilon}_0))}{\rho c \theta_m} - \frac{C}{1 + C \ln(\dot{\epsilon}_i/\dot{\epsilon}_0)} = 1. \quad (5)$$

The instability strains computed from Eq. (5) are also listed in Table 3. There is very little difference between the instability strains predicted from Eqs. (3) and (5) primarily because of weak strain-rate hardening of the materials considered.

Note that we have studied plane strain transient deformations, and σ_{11} , σ_{12} and σ_{33} do not vanish as they do in a simple tension test. Thus the average axial strain predicted by the Considère condition need not equal that when the maximum shear stress attains its peak value. The reduction in the area of cross-section is included in the derivation of Eqs. (3) and (5) and is also considered in the plane strain deformations of the specimen. It is clear from values listed in Table 3 that the effective plastic strain predicted from the Eqs. (3) and (5) differs significantly from the effective plastic strain at the time of initiation of an ASB. Furthermore, the Considère criterion does not accurately predict the ordering of materials according to the ASB initiation time under otherwise identical conditions. Batra et al. (1995) numerically studied 3-D torsional deformations of a thin-walled tube made of each of these 11 materials. The prescribed tangential velocity at the end faces of the tube produced an average shear strain rate of 5000/s. When ranked according to the average shear strain at the time of initiation of an ASB, the order determined by Batra et al. (1995) is: Tungsten, S-7 tool steel, Depleted Uranium, 2024-T351 aluminum, 7039-aluminum, 4340 steel, Armco iron, Carpenter Electric iron, 1006 steel, Cartridge brass, and OFHC Copper. It differs from that presently found and listed in column 1 of Table 3 suggesting that the ranking depends upon the type of test and/or the state of stress.

3.7. Evolution of porosity and temperature

The time histories of the evolution of the maximum shear stress, the effective plastic strain ϵ_p^e , the porosity f and the temperature θ at the centroid of the cross-section are plotted in Fig. 5(a)–(d). Oscillations in the maximum shear stress vs. the nondimensional time curves are due to the interaction among the incident and the reflected waves. These oscillations are predominant in materials having a small value of A/ρ such as the cartridge brass, copper, the carpenter electric iron, Armco iron and 1006

steel. The value of the quasistatic yield stress A is low for these materials; thus, plastic deformations ensue virtually instantaneously upon the arrival at the centroid of the initial tensile loading wave. This results in a sharp increase in the effective plastic strain and the porosity until the strain hardening effects and the compressive wave reflected from the top surface neutralize the effect of the initial tensile loading wave. Subsequent growth rate of f , ε_c^p and θ is consistent with that for the other six materials. The time of initiation of an ASB could also be identified as the instant when $\dot{\varepsilon}_c^p$ suddenly increases, but this criterion is difficult to implement in a computer code. Test observations on materials deformed under shock loading have revealed that a material point fails when the porosity there equals 0.25. With this failure criterion, depleted uranium, tungsten heavy alloy and S-7 tool steel will fail in plane strain tensile deformations at a nominal axial strain of about 0.14. The carpenter electric iron and the Armco iron will fail at an average axial strain of 0.45 which is higher than that for copper; these values depend upon the assumed initial porosity distribution. Due to a lack of the test data, values of material parameters in the equation giving the evolution of porosity have been taken to be the same for the eleven materials. Thus the computed failure strains should not be expected to match very well with experimental findings. Here, ε_c^p has exceeded ε_n for each of the eleven materials studied, therefore, significant nucleation of new voids has occurred; ε_n equals the effective plastic strain when voids begin to nucleate. The nondimensional temperature in Fig. 5(d) is the homologous temperature. These plots reveal that the maximum value of the homologous temperature is 0.4; thus thermal softening has not been very significant.

3.8. Comparison of ASB initiation time with that given by the Considère condition

In order to vividly illustrate the differences among the strains predicted by the Considère condition, when the maximum shear stress peaks and when an ASB initiates, we have plotted in Fig. 6 the axial load vs. the non-dimensional time for the 4340 steel, 7039 aluminum and OFHC copper. It is clear that in the 4340 steel and 7039 aluminum, the load begins to drop severely at the instant of the initiation of the ASB; however, for copper the drop in the axial load subsequent to the initiation of the ASB is negligible. For each one of the three materials, the axial strain predicted by the Considère condition is considerably smaller than that when the maximum shear stress peaks even though the decrease in the cross-sectional area during loading has been accounted for in the Considère condition.

3.9. Effect of thermal conductivity

Batra and Kim (1991) have analyzed the effect of thermal conductivity κ on the initiation and development of an ASB in a thermoviscoplastic material deformed in simple shear. They found that it virtually has no effect on the time of initiation of an ASB but strongly influences the development of the ASB. Batra and Chen (2001a) found that during the final stage of the development of an ASB in a 4340 steel, 85% of the heat produced due to plastic working is conducted out of the

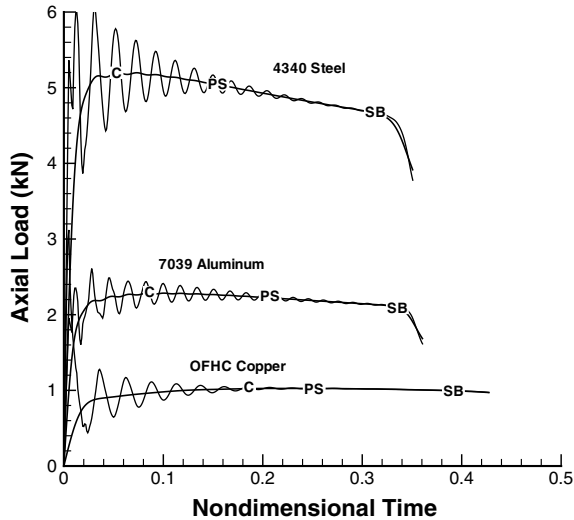


Fig. 6. Axial load vs. the effective plastic strain for 4340 steel, 7039 aluminum, and OFHC copper with the effective plastic strain from the Considerè condition (C), at the peak maximum shear stress (PS), and at shear band initiation (SB) indicated.

ASB edges. Here we examine the effect of thermal conductivity in a 2-D problem on the initiation and propagation of an ASB in copper and 4340 steel. For each material, the problem was analyzed again by setting $\kappa = 0$. As is evident from the plots in Fig. 7 of the ASB length vs. time, the initiation and the speed of propagation of an ASB in the 4340 steel for both $\kappa = 0$ and $\kappa > 0$ are essentially the same. However, in copper, the initiation time of the ASB is decreased by about 4% with $\kappa = 0$, and the initial and the final propagation speeds increase by 1.4% and 6.5%, respectively. The two time histories of the maximum shear stress revealed that the thermal conductivity significantly affects the rate of collapse of the shear stress after the band has initiated and hence its formation/development; similar results were obtained by Batra and Kim (1991) for simple shearing deformations with the Bodner-Partom (1975) thermoviscoplastic relation.

3.10. Effect of nominal strain-rate

For the 4340 steel, the weak defect and for four values of the average axial strain rate, Fig. 8(a) and (b) exhibits time histories of the evolution of the maximum shear stress at the centroid of the cross-section and of the ASB length. The nominal strain rate was varied by changing the steady value of the axial velocity applied on the top and the bottom surfaces. The rise time t_r of the prescribed axial velocity was increased from 1 to 5 μs in order to successfully compute results for the highest axial strain rate considered; $t_r = 5 \mu\text{s}$ was used for each of the four cases. As expected, the initiation of an ASB is significantly delayed with an increase in the axial strain rate; a

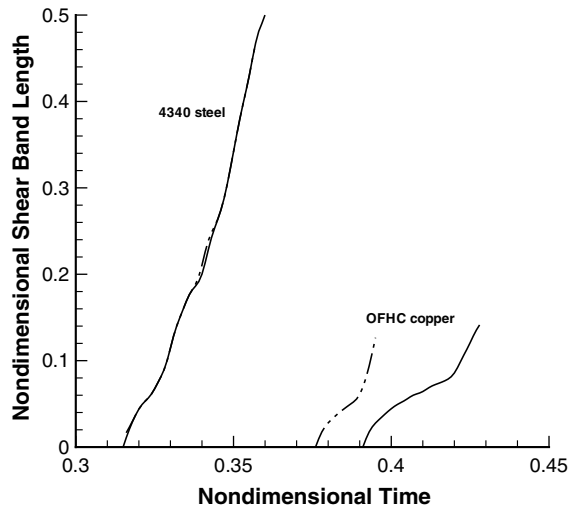


Fig. 7. Time histories of the length of the shear band for OFHC copper and 4340 steel; the solid and the dashed lines are respectively with and without the effects of heat conduction.

similar result for the simple shear problem was obtained by Batra (1988a,b). The drop in the maximum shear stress is less precipitous at the axial strain rate of 40,000/s as compared to that at the axial strain rate of 2000/s. Also, the initial ASB speed drops with an increase in the axial strain rate, but the final ASB speed is essentially independent of the applied axial strain rate. The computed shear band speeds for the four axial strain rates are listed in Table 4. For the torsional deformations of a thin-wall tube, Batra and Zhang (1994) found that the initial speed of an ASB increased from 250 m/s at a nominal shear strain rate of 5000/s to 1000 m/s when the nominal shear strain rate equalled 25,000/s. In the torsional problem, the shear band propagates along the circumference of the tube and that is also the loading direction; its propagation is not restrained by the deformed material surrounding the ASB tip. However, in the plane strain tension problem, the ASB propagates along a direction that makes an angle of about 45° with the loading axis. The initial speed of the ASB decreases with an increase in the nominal axial strain rate, but the final speed is essentially the same.

3.11. Variation of effective plastic strain rate along an ASB

Fig. 9(a) depicts, at three different instants of time during the development, the distribution of the effective plastic strain rate along an ASB in the 4340 steel. The tip of the ASB, marked with a vertical line, moves at an average speed of approximately 300 m/s. At the tip of the band the effective plastic strain rate has the maximum value of $10^5/s$ and the effective plastic strain has the minimum value. As the band develops, the effective plastic strain rate ahead of the band becomes uniform and nearly equals that at the ASB tip. During the early stage of the development

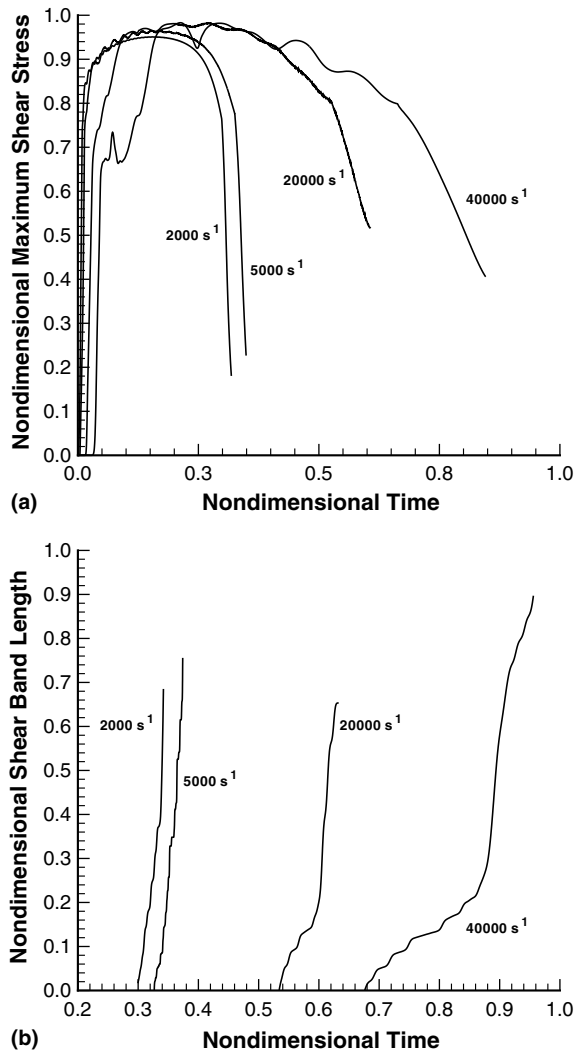


Fig. 8. For the 4340 steel using four values of the applied axial strain rate, time histories of (a) the evolution of the maximum shear stress, and (b) the length of the ASB.

of an ASB, the gradient of the effective plastic strain rate along the band is lower ahead of the band tip than that behind it.

3.12. Remarks

Whereas the ASB initiation time is relatively unaffected (cf. Table 1) by the FE mesh employed, the same can not be said about the ASB width. Postlocalization computations with the 120×120 uniform mesh could not be performed because of

Table 4

The ASB initiation times, and initial and final speeds of the ASB for four values of the average axial strain rate

Average axial strain rate (1/s)	Nondimensional ASB initiation time	Initial ASB speed (m/s)	Final ASB speed (m/s)
2000	0.300	245	243
5000	0.327	214	252
20,000	0.534	136	276
40,000	0.676	50	246

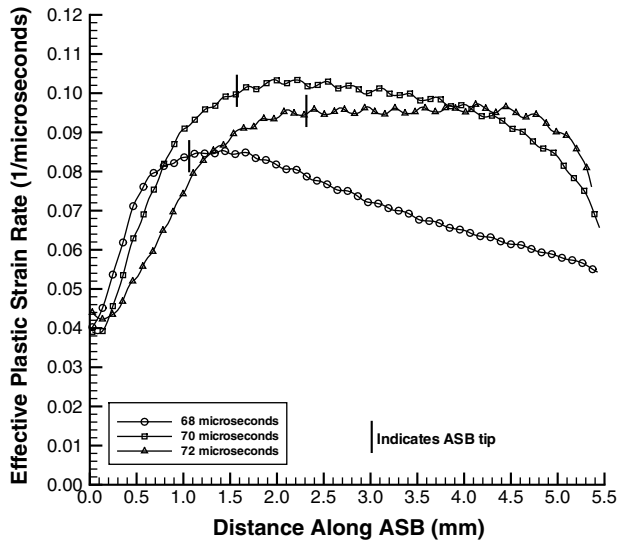


Fig. 9. Variation of the effective plastic strain rate along an ASB in the 4340 steel.

the enormous CPU time and storage required. One way to obtain mesh-independent results is to use a strain-rate gradient-dependent theory, e.g. see [Batra \(1987a,b\)](#), [Batra and Kim \(1990b\)](#) and [Batra and Hwang \(1994\)](#). Such theories involve a material characteristic length and third-order spatial gradients of displacements or velocities in the problem formulation thereby necessitating the use of either Hermitian basis functions or auxiliary variables. At present, to our knowledge, there are no good ways of estimating the material characteristic length. Furthermore, these theories may either not give a finite speed of elastic waves or a unique solution of the linear elastic problem; see [Batra \(1975\)](#) for the corresponding thermal problem. [Batra and Chen \(1999\)](#), and [Chen and Batra \(1999b\)](#) employed a strain-rate-gradient dependent plasticity theory to find spacing between adjacent ASBs. Alternatively, one can use an adaptively refined mesh to delineate the width of an ASB; e.g. see [Batra and Ko \(1992, 1993\)](#). Frequent remeshing smoothens out the deformation fields and consequently delays the initiation of an ASB. Another possibility is to use a meshless

method such as the modified smooth particle hydrodynamics (Batra and Zhang (2004)).

Here we have used the Johnson-Cook (1983) relation to represent the thermoviscoplastic behavior of the material because of the availability of values of material parameters. Batra and Kim (1990a,b) used four thermoviscoplastic relations, namely, the Johnson-Cook, Bodner-Partom (1975), the Litonski-Batra (e.g. see Batra (1988a,b)) and a power law. These relations were calibrated to give nearly the same shear stress vs. the shear strain curve during homogeneous deformations of the body. However, during inhomogeneous deformations, these gave qualitatively similar but quantitatively different results, and predicted different ASB initiation times and postlocalization behaviors.

4. Conclusions

We have analyzed the problem of the initiation and propagation of an ASB in plane strain coupled thermomechanical deformations of a microporous, isotropic and homogeneous thermoviscoplastic material with a hyperbolic heat equation. For uniform 40×40 and 120×120 finite element meshes, the ASB initiation time differed by 2.1%. The nominal strain at which an ASB initiates and its speed of propagation have been ascertained for eleven materials, namely, depleted uranium, tungsten, S-7 tool steel, 4340 steel, 7039 aluminum, 2024 aluminum, 1006 steel, OFHC copper, cartridge brass, carpenter electric iron and armco iron. These materials are listed in the order of their decreasing susceptibility to adiabatic shear banding. This ranking is unaffected by the defect size. The same defect, in terms of a nonuniform distribution of initial porosity, was introduced in each of the eleven materials. The presently found ranking of materials according to their susceptibility to adiabatic shear banding is different from that found earlier by Batra et al. (1995) who analyzed their simple shearing deformations.

For the 4340 steel, a parametric study has been conducted for seven values of the thermal wave speed. The initiation time of an ASB is noticeably affected by the thermal wave speed only when the wave speed drops down from infinity to a few m/s. For the 4340 steel and the OFHC copper, results have been computed with and without the effects of heat conduction. It is found that the assumption of locally adiabatic deformations does not influence the initiation time and the speed of an ASB in the 4340 steel; however, it does so in the copper. During the development of the ASB in copper, the rate of drop of the maximum shear stress is much higher for locally adiabatic deformations as compared to that when heat conduction is considered. Batra and Chen (2001a) found that during the late stages of the development of an ASB, nearly 85% of the heat produced due to plastic working is conducted out of the edges of the band. Thus heat conduction influences the band width and the time elapsed between the initiation and the full development of the band.

The initial speed of propagation of an ASB is found to decrease and its time of initiation increase with an increase in the nominal axial strain rate; however, the final speed of propagation of the band is unaffected by the nominal axial strain rate. Dur-

ing torsional deformations of a thin-wall tube, Batra and Zhang (1994) found that the ASB speed increased with an increase in the nominal strain rate.

Considerable porosity evolved during the development of an ASB. For some materials it exceeded the value believed to induce ductile failure; however, no failure was simulated.

Acknowledgments

This work was partially supported by the NSF Grant CMS0002849, the ONR Grant N00014-98-1-0300 and N00014-03-MP-2-0131, the ARO Grant DAAD19-01-1-0657, and the AFOSR MURI subcontract from Georgia Institute of Technology to Virginia Polytechnic Institute and State University. Opinions expressed in the paper are those of the authors and not of funding agencies.

References

- Armstrong, R., Batra, R.C., Meyers, M., Wright T.W., (Eds.), 1994. Shear Instabilities and Viscoplasticity Theories, A Special Issue of the *Mechanics of Materials Journal*, 17, pp. 83–328.
- Bai, Y.L., 1982. Thermoplastic instability in simple shear. *Mech. Phys. Solids* 30, 195–207.
- Bai, Y.L., Dodd, B., 1992. *Adiabatic Shear Localization: Occurrence, Theories, and Applications*. Pergamon Press.
- Batra, R.C., 1975. On heat conduction and wave propagation in non-simple rigid solids. *Lett. Appl. Eng. Sci.* 3, 97–107.
- Batra, R.C., 1987a. Effect of material parameters on the initiation and growth of adiabatic shear bands. *Int. J. Solids Struct.* 23, 1435–1446.
- Batra, R.C., 1987b. The initiation and growth of, and the interaction among adiabatic shear bands in simple and dipolar materials. *Int. J. Plasticity* 3, 75–89.
- Batra, R.C., 1988a. Effect of nominal strain-rate on the Initiation and growth of adiabatic shear bands in steels. *J. Appl. Mech.* 55, 229–230.
- Batra, R.C., 1988b. Steady state penetration of thermoviscoplastic targets. *Comp. Mech.* 3, 1–12.
- Batra, R.C., Kim, K.H., 1990a. Effect of viscoplastic flow rules on the Initiation and growth of shear bands at high strain rates. *J. Mech. Phys. Solids* 38, 859–874.
- Batra, R.C., Kim, C.H., 1990b. Adiabatic shear banding in elastic–viscoplastic nonpolar and dipolar materials. *Int. J. Plasticity* 6, 127–141.
- Batra, R.C., Kim, C.H., 1991. Effect of thermal conductivity on the initiation and growth of adiabatic shear bands in steels. *Int. J. Eng. Sci.* 29, 949–960.
- Batra, R.C., Kim, C.H., 1992. Analysis of shear banding in twelve materials. *Int. J. Plasticity* 8, 425–452.
- Batra, R.C., Ko, K.I., 1992. An adaptive mesh refinement technique for the analysis of shear bands in plane strain compression of a thermoviscoplastic solid. *Comput. Mech.* 10, 369–379.
- Batra, R.C., Ko, K.I., 1993. Analysis of shear bands in dynamic axisymmetric compression of a thermoviscoplastic cylinder. *Int. J. Eng. Sci.* 31, 529–547.
- Batra, R.C., Hwang, J., 1994. Dynamic shear band development in dipolar thermoviscoplastic materials. *Comput. Mech.* 12, 354–369.
- Batra, R.C., Jin, X.S., 1994. Analysis of Dynamic Shear Bands in Porous Thermally Softening Viscoplastic Materials. *Arch. Mech.* 46, 13–36.
- Batra, R.C., Zbib, H.M., 1994. *Material Instabilities: Theory and Applications*. ASME Press.
- Batra, R.C., Zhang, X., 1994. On the propagation of a shear band in a steel tube. *J. Eng. Mat. Tech.* 116, 155–161.

- Batra, R.C., Zhang, X., Wright, T.W., 1995. Critical strain ranking of 12 materials in deformations involving adiabatic shear bands. *J. Appl. Mech.* 652, 252–255.
- Batra, R.C., Liang, X.Q., 1997. Finite dynamic deformations of smart structures. *Comput. Mech.* 20, 427–438.
- Batra, R.C., Rattazzi, D., 1997. Adiabatic shear banding in a thick-walled steel tube. *Comput. Mech.* 5, 426–442.
- Batra, R.C., 1998. Numerical solution of initial-boundary-value problems with shear strain localization. In: Perzyna, P. (Ed.), *Localization and Fracture Phenomenon in Inelastic Solids*. Springer, Wien, pp. 301–389.
- Batra, R.C., Chen, L., 1999. Shear band spacing in gradient-dependent thermoviscoplastic materials. *Comput. Mech.* 23, 8–19.
- Batra, R.C., Rajapakse, Y.D.S., Rosakis, A., 2000. Failure mode transitions under dynamic loading. *Int. J. Fracture* 101, 1–180 (special issue).
- Batra, R.C., Ravisankar, M.V.S., 2000. Three-dimensional numerical simulation of the Kalthoff experiment. *Int. J. Fracture* 105, 161–186.
- Batra, R.C., Chen, L., 2001a. Effect of viscoplastic relations on the instability strain, shear band initiation strain, the strain corresponding to the maximum shear band spacing, and the band width in a thermoviscoplastic material. *Int. J. Plasticity* 17, 1465–1489.
- Batra, R.C., Chen, L., 2001b. Instability analysis and shear band spacing in gradient-dependent thermoviscoplastic materials with finite speeds of thermal waves. *Arch. Mech.* 53, 167–192.
- Batra, R.C., Jaber, N.A., 2001. Failure mode transition in an impact loaded prenotched plate with four thermoviscoplastic relations. *Int. J. Fracture* 110, 47–71.
- Batra, R.C., Wang, Z., 2004. Failure mode transition speed in three-dimensional transient deformations of microporous heat-conducting thermoelastoviscoplastic prenotched plate, submitted for publication.
- Batra, R.C., Love, B.M., 2004. Adiabatic shear bands in functionally graded materials. *J. Thermal Stresses* 27, 1101–1123.
- Batra, R.C., Lear, M.H., 2004. Simulation of brittle and ductile fracture in an impact loaded prenotched plate. *Int. J. Fracture* 126, 179–203.
- Batra, R.C., Zhang, G.M., 2004. Analysis of adiabatic shear bands in elasto-thermo-viscoplastic materials by modified smoothed-particle hydrodynamics (MSPH) method. *J. Comput. Phys.* 201, 172–190.
- Bodner, S.R., Partom, Y., 1975. Constitutive equations for elastic–viscoplastic strain-hardening materials. *J. Appl. Mech.* 56, 385–389.
- Bonnet-Lebouvier, A.-S., Mollinari, A., Lipinski, P., 2002. Analysis of dynamic propagation of adiabatic shear bands. *Int. J. Solids Struct.* 39, 4249–4269.
- Burns, T.J., Davies, M.A., 2002. On repeated adiabatic shear band formation during high-speed machining. *Int. J. Plasticity* 18, 487–506.
- Chandrasekharai, D.S., 1986. Thermoelasticity with second sound: A review. *Appl. Mech. Rev.* 39, 355–376.
- Charalambakis, N., Baxevanis, T., 2004. Adiabatic shearing of non-homogeneous thermoviscoplastic materials. *Int. J. Plasticity* 20, 899–914.
- Chen, L., Batra, R.C., 1999a. The asymptotic structure of a shear band in mode-II deformations. *Int. J. Eng. Sci.* 37, 895–919.
- Chen, L., Batra, R.C., 1999b. Effect of material parameters on shear band spacing in work-hardening gradient-dependent thermoviscoplastic materials. *Int. J. Plasticity* 15, 551–574.
- Chu, C., Needleman, A., 1980. Void nucleation effects in biaxially stretched sheets. *J. Eng. Mater. Technol.* 102, 249–256.
- Clifton, R.J., 1980. Adiabatic shear in material response to ultrahigh loading rates. In: Herrmann, W., et al. (Eds.), *NRC National Material Advisory Board (U.S.) Report NMAB-36*, Washington, DC.
- Considère, A.G., 1885. Memiore sur L'emploi du fer et de L'acier dans les constructions. *Annals des Ponts et Chaussées* 9, 574–775.
- Gurson, A.L., 1977. Continuum theory of ductile rupture by void nucleation and growth: Part I. *J. Eng. Mater. Technol.* 99, 2–15.
- Hart, E.W., 1967. Theory of the tensile test. *Acta Metall.* 15, 351–355.

- Johnson, G.R., Cook, W.H., 1983. A constitutive model and data for metals subjected to large strains, high strain-rates, and high temperatures. In: *Proceedings of the 7th International Symposium on Ballistics*, pp. 541–547.
- Lear, M.H., 2003. Numerical simulation of adiabatic shear bands and crack propagation in thermoviscoplastic materials, Doctoral dissertation, Virginia Polytechnic Institute and State University, Blacksburg, VA.
- Lindholm, U.S., Johnson, G.R., 1983. Material behavior under high stress and ultrahigh loading rates. *Sagamore Army Mater. Research Conf.* 29, 61–79.
- Marchand, A., Duffy, J., 1988. An experimental study of the formation process of adiabatic shear bands in a structural steel. *J. Mech. Phys. Solids* 36, 251–283.
- Mason, J.J., Rosakis, A.J., Ravichandran, G., 1994. On the strain and strain rate dependence of the fraction of plastic work converted to heat: An experimental study using high speed infrared detectors and Kolsky bar. *Mech. Mater.* 17, 135–146.
- Massey, H.F., 1928. The flow of metal during forging. In: *Proc. Manchester Assoc. of Engineers*, pp. 21–26.
- Molinari, A., Clifton, R.J., 1987. Analytical characterization of shear localization in thermoviscoplastic materials. *J. Appl. Mech.* 54, 806–812.
- Molinari, A., Musquar, C., Sutter, G., 2002. Adiabatic shear banding in high speed machining of Ti-6Al-4V: experiments and modeling. *Int. J. Plasticity* 18, 443–459.
- Needleman, A., 1989. Dynamic shear band development in plane strain. *J. Appl. Mech.* 56, 1–6.
- Perzyna, P. (Ed.), 1998. *Localization and Fracture Phenomenon in Inelastic Solids*. Springer, Wien, NY.
- Recht, R.F., 1964. Catastrophic thermoplastic shear. *J. Appl. Mech.* 31, 189–193.
- Saad, M.H., Cha, C.Y., 1982. Axisymmetric non-Fourier temperature in cylindrically bounded domains. *Int. J. Nonlinear Mech.* 17, 129–136.
- Schoenfeld, S.E., Kad, B., 2002. Texture effects on shear response in Ti-6Al-4V plates. *Int. J. Plasticity* 18, 461–486.
- Taylor, G.I., Quinney, H., 1934. The latent energy remaining in a metal after cold working. *Proc. Royal Soc. A* 143, 307–326.
- Tresca, H., 1878. On further application of the flow of solids. *Proc. Inst. Mech. Engrs.* 30, 301–345.
- Tvergaard, V., Needleman, A., 1984. Analysis of the cup-cone fracture in a round tensile bar. *Acta Metall.* 32, 157–169.
- Vandergiesen, E., Vanderburg, M.W.D., Needleman, A., Tvergaard, V., 1995. Void growth due to creep and grain-boundary diffusion at high triaxialities. *J. Mech. Phys. Solids* 43, 123–165.
- Vernotte, P., 1958. The true heat equation. *CR Acad. Sci.* 247, 2103.
- Wei, Z., Batra, R.C., 2002. Dependence of instability strain upon damage in thermoviscoplastic materials. *Arch. Mech.* 54, 691–707.
- Wright, T.W., Walter, J.W., 1996. The asymptotic structure of an adiabatic shear band in antiplane motion. *J. Mech. Phys. Solids* 44, 77–97.
- Wright, T.W., 2002. *The Physics and Mathematics of Adiabatic Shear Bands*. Cambridge University Press.
- Wright, T.W., Batra, R.C., 1985. The initiation and growth of adiabatic shear bands. *Int. J. Plasticity* 1, 205–212.
- Zbib, H.M., Shawki, T., Batra, R.C. (Eds.), 1992. *Material Instabilities*. *Appl. Mech. Rev.*, 45, pp. 1–173 (special issue).
- Zbib, H.M., Jubran, J.S., 1992. Dynamic shear banding – a 3-dimensional analysis. *Int. J. Plasticity* 8, 619–641.
- Zener, C., Hollomon, J.H., 1944. Effect of strain rate upon plastic flow of steel. *J. Appl. Phys.* 15, 22–32.
- Zhou, M., Ravichandran, G., Rosakis, A., 1996a. Dynamically propagating shear bands in impact-loaded prenotched plates – I. *J. Mech. Phys. Solids* 44, 981–1006.
- Zhou, M., Ravichandran, G., Rosakis, A., 1996b. Dynamically propagating shear bands in impact-loaded prenotched plates – II. *J. Mech. Phys. Solids* 44, 1007–1032.
- Zhu, Z., Batra, R.C., 1991. Shear band development in a thermally softening viscoplastic body. *Comput. Struct.* 39, 459–472.